Eur. Phys. J. A **2**, 337–342 (1998)

THE EUROPEAN PHYSICAL JOURNAL A

Short note

Electron screening in backward elastic scattering*

F. Schümann[1], S. Zavatarelli[2], L. Gialanella[1], U. Greife[1], M. Junker[1,3], D. Rogalla[1], C. Rolfs[1], F. Strieder[1], H.P. Trautvetter[1]

[1] Institut für Physik mit Ionenstrahlen, Ruhr-Universität, Bochum, Universitätsstr. 150, D-44780 Bochum, Germany
[2] Dipartimento di Fisica, Università di Genova and INFN, Via Dolecaneso, I-16146 Genova, Italy
[3] Laboratori Nazionali del Gran Sasso, I-67010 Assergi, Italy

Received: 25 May 1998
Communicated by B. Povh

Abstract. The elastic scattering cross sections, $\sigma(E,\theta)$, for the systems He+Ta and He+W have been measured at $\theta_{lab} = 165^\circ$ and $E_{lab} = 76.1$ keV to 3.988 MeV using targets with a thickness of a few atomic layers. The results are smaller than the results given by the Rutherford scattering law, $\sigma_R(E,\theta)$, due to the effects of electron screening and can be described by $\sigma(E,\theta)/\sigma_R(E,\theta) = (1 + U_e/E)^{-1}$, where U_e is an atomic screening potential energy. The deduced average value, $U_e = 28 \pm 3$ keV, is consistent with the Moliére- and Lenz-Jensen-models as well as electron binding energies.

PACS. 25.60.Bx Elastic scattering

1 Introduction

Accurate knowledge of thermonuclear reaction rates is important for the field of nuclear astrophysics [1,2]. Due to the Coulomb barrier E_c of the entrance channel, the cross section $\sigma(E)$ of these charged-particle-induced reactions drops nearly exponentially with decreasing energy E, thus it becomes increasingly difficult to measure $\sigma(E)$. As a consequence, the observed energy dependence $\sigma(E)$ at higher energies must be extrapolated to the thermal energy region in stars. The extrapolation is facilitated if the cross-section data are transformed into the astrophysical $S(E)$ factor, conventionally defined by the equation

$$\sigma(E) = S(E)E^{-1}\exp(-2\pi\eta), \qquad (1)$$

where η is the Sommerfeld parameter given by $2\pi\eta = 31.29 Z_1 Z_2 (\mu/E)^{1/2}$. The quantities Z_1 and Z_2 are the integral nuclear charges of the interacting particles in the entrance channel, μ is the reduced mass in units of amu, and E is the center-of-mass energy in units of keV.

In the extrapolation of $\sigma(E)$ using (1), it is assumed that the Coulomb potential of the target nucleus and projectile is that resulting from bare nuclei. However, for nuclear reactions studied in the laboratory, the target nuclei and the projectiles are usually in the form of neutral atoms / molecules and ions, respectively. The electron clouds surrounding the interacting nuclides act as a screening potential: the projectile effectively sees a reduced Coulomb barrier. This in turn leads to a higher cross section, $\sigma_s(E)$, than would be the case for bare nuclei, $\sigma_b(E)$. There is an enhancement factor [3]

$$f_{lab}(E) = \sigma_s(E)/\sigma_b(E) \approx \exp(\pi\eta \mathrm{U_e/E}), \qquad (2)$$

where U_e is the electron-screening potential energy (e.g., $U_e \approx Z_1 Z_2 e^2/R_a$ approximately, with R_a an atomic radius). Note that $f_{lab}(E)$ increases exponentially with decreasing energy. For ratios $E/U_e > 1000$, shielding effects are negligible, and laboratory experiments can be regarded as essentially measuring $\sigma_b(E)$. However, for $E/U_e < 100$, shielding effects become important for understanding and extrapolating low-energy data. Relatively small enhancements from electron screening at energy ratios $E/U_e \approx 100$ can cause significant errors in the extrapolation of cross sections to lower energies, if the curve of the cross section is forced to follow the trend of the enhanced cross sections, without correction for the screening. Notice that for a stellar plasma, the value of $\sigma_b(E)$ must be known because the screening in the plasma can be quite different from that in the laboratory nuclear-reaction studies, and $\sigma_b(E)$ must be explicitly included for each situation. Thus, a good understanding of electron-screening effects is needed to arrive at reliable $\sigma_b(E)$ data at low energies. Experimental studies of fusion reactions involving light nuclides [4-10] have shown the expected exponential enhancement of the cross section at low energies. However, the observed enhancement was in all cases signifi-

* Supported in part by the Deutsche Forschungsgemeinschaft Ro429/28-1 and INFN

cantly larger than could be accounted for from available atomic-physics models [11-14]. The situation is disturbing because if the effects of electron screening are not understood under laboratory conditions, they are most likely also not understood in a stellar plasma. A solution to the above puzzle might be found in one (or all) of the following areas: (i) the assumed energy-loss predictions at low energies (see [15] for the case of the d+^{3}He system), (ii) the assumed nuclear-reaction models at energies far below E_c, and (iii) the assumed atomic-physics models. All areas demand for additional experimental efforts. A possible way to test area (iii) is to study the elastic scattering at backward angles and at energies far below E_c, since the process should be influenced here only by atomic physics.

The observed number of scattered projectiles per unit of time in a given detector, $N(E_{lab}, \theta_{lab})$, is related to the elastic scattering cross section in the center-of-mass system, $\sigma(E, \theta)$, by the equation

$$N(E_{lab}, \theta_{lab}) = N_p N_t \sigma(E, \theta)(\Omega_{cm}/\Omega_{lab}) d\Omega_{lab}, \quad (3)$$

where N_p is the number of incident projectiles per unit of time, N_t is the number of target atoms per unit area, Ω_{cm}/Ω_{lab} is the ratio of solid angles between the center-of-mass and laboratory systems, and $d\Omega_{lab}$ is the solid angle of the detector in the laboratory frame. The energy E is the effective energy within the target thickness. The screening factor for elastic scattering is given by

$$f_{lab}(E, \theta) = \sigma(E, \theta)/\sigma_R(E, \theta), \quad (4)$$

where $\sigma_R(E, \theta)$ is the Rutherford scattering cross section

$$\sigma_R(E, \theta) = 1.296 Z_1 Z_2 E^{-2} \sin^{-4}(0.5\theta) \ \ [\text{mb/sr}]. \quad (5)$$

Previous work suggested [26 and references therein] - as a first order approximation at backward angles - an angle-independent screening factor of the form

$$f_{lab}(E, \theta) = (1 + U_e/E)^{-1}. \quad (6)$$

Several groups have performed basic studies on the screening effects in elastic scattering [16-30]. These studies fall roughly into one of two groups: those performed at relatively low energy [16-20], where the screening factor $f_{lab}(E, \theta)$ is less than about 0.85 ("strong screening"), and those performed at higher energy [21-30], where the screening factor is greater than about 0.85 ("weak screening"). Experimental results and calculations of the screened cross sections are generally in good agreement for the high energy group of studies. In marked contrast, lower energy studies have typically observed weaker screening than predicted by theory, and the results of these studies do not smoothly join with results obtained at higher energy.

As a first step in the puzzle discussed above and in order to have data of electron screening effects over a wide and continuous range of energies (covering the transition from low to high energies), we report on results obtained for the scattering systems ^{4}He+^{181}Ta (E_c = 20.7 MeV) and ^{4}He+^{184}W (E_c = 20.3 MeV) at $\theta_{lab} = 165°$ and E_{lab} = 76.1 keV to 3.988 MeV using targets with a thickness of a few atomic layers. Assuming U_e = 30 keV (section 3) one finds $f_{lab}(E, \theta)$ = 0.72 and 0.992 at E_{lab} = 76.1 keV and 3.988 MeV, respectively. Thus, the cross section $\sigma(E, \theta)$ must be determined via eq. (3) with an absolute precision of a few percent. To achieve this precision, all previous studies performed relative measurements, e.g. using mixed targets (with light and heavy components), where the high-energy data (for which the screening effects are negligible) were normalized to $\sigma_R(E, \theta)$ for both target components. We followed a similar procedure by normalising the data to $\sigma_R(E, \theta)$ at the highest energy, corrected by the 0.8% electron screening effects. Details not reported here can be found in [31].

2 Apparatus and experimental procedures

The 4 MV Dynamitron tandem accelerator at Bochum provided a ^{4}He beam in the energy range E_{lab} = 0.25 to 3.988 MeV with currents from 3 to 40 nA, respectively. The absolute beam energy is known to a precision of $1.4 \cdot 10^{-4}$ [32], leading to a negligible error of 0.03% in $\sigma(E, \theta)$ at E_{lab} = 0.25 MeV. The ^{4}He beam from the 400 kV single stage accelerator - interconnected with the tandem beam lines - was used at E_{lab} = 76.1 to 400 keV (with currents below 5 nA); its absolute energy was calibrated in the course of this experiment and is known to a precision of better than 0.4 keV, leading to a 1.1% error in $\sigma(E, \theta)$ at E_{lab} = 76.1 keV.

The beam entered a cylindrical scattering chamber (inner diameter = 431 mm, height = 114 mm) through 2 apertures (A_1 and A_2) and was stopped in the target, which was placed at the center of the chamber (target-normal parallel to the beam direction). The apertures (2.0 mm diameter) were installed at respective distances of 100 and 720 mm from the target and defined the beam direction to better than 0.18° (beam spot on target: less than 2.6 mm diameter). The uncertainty in beam direction leads to a negligible error in $\sigma(E, \theta)$ (less than 0.08%). The target was surrounded by an electrically insulated cylindrical chamber (170 mm diameter, 80 mm height) with 12 mm diameter holes for the beam entrance and for viewing the target from the detector positions. This inner chamber together with the target served as the Faraday cup for beam integration. The area of the holes relative to the total area of the chamber is 0.9%, which represents the maximum loss of secondary electrons produced at the target. In order to suppress also the influence of secondary electrons produced by the incident beam on the apertures A_1 and A_2, another aperture with 10 mm diameter was placed between the apertures (at a 215 mm distance from the target) followed by an electrically insulated tube (12 mm diameter, 98 mm length), which housed the aperture A_2 together with a 3 mm diameter aperture (5 mm downstream); a negative voltage of 300 V was applied to the latter aperture. The current integrator was calibrated using a constant current source leading to a precision of 0.35%. In order to minimise carbon deposition on the target, the top part of the inner chamber

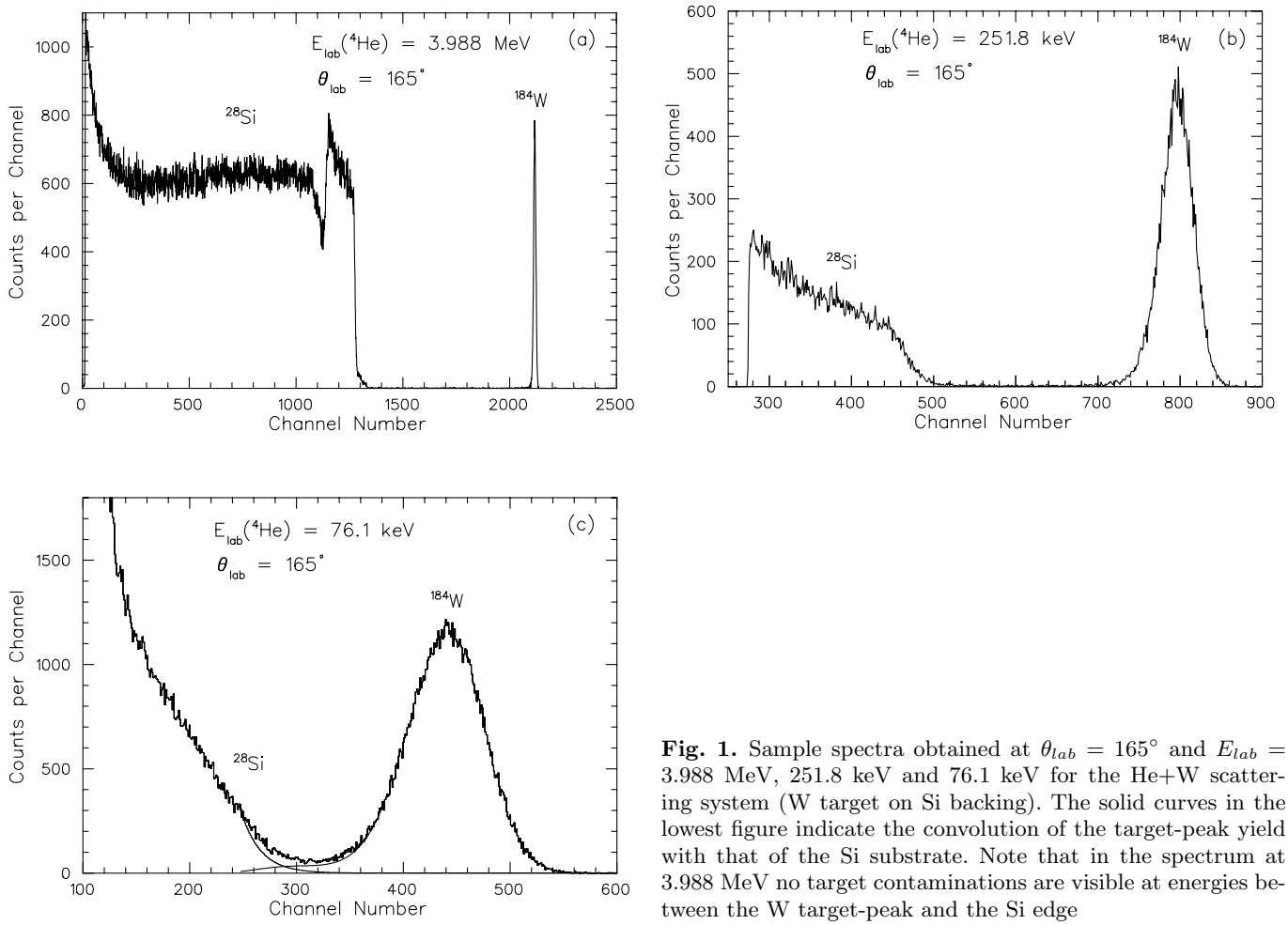

Fig. 1. Sample spectra obtained at $\theta_{lab} = 165°$ and $E_{lab} =$ 3.988 MeV, 251.8 keV and 76.1 keV for the He+W scattering system (W target on Si backing). The solid curves in the lowest figure indicate the convolution of the target-peak yield with that of the Si substrate. Note that in the spectrum at 3.988 MeV no target contaminations are visible at energies between the W target-peak and the Si edge

consisted of a flat Cu-disk cooled to liquid nitrogen temperature, which led to a pressure of $6 \cdot 10^{-7}$ mbar in the chamber. Measurements using the ^{12}C(d,p)^{13}C reaction at $E_d = 920$ keV have shown [31] that carbon-deposition on the targets was negligible. Two Si-surface-barrier detectors (100 μm thickness, 25 mm^2 active area, 20 keV energy resolution at $E_\alpha = 5.5$ MeV, 0.029 μm thick Au surface layer) were placed at the symmetric angles $\theta_{lab} = 165°$ and $-165°$ (each at a distance of 163.0 ± 1.5 mm), in order to compensate for the effects of beam shifts on target. They were mounted (electrically insulated) at the end of 75 mm long pipes, which in turn were fixed at the outer wall of the inner chamber. Each detector was collimated by an aperture of 2.95 ± 0.05 mm diameter placed in front of the detector; the setup led to a solid angle of $d\Omega_{lab} = (2.57 \pm 0.13) \cdot 10^{-4}$ sr and to a maximum uncertainty in angle position of 1°. Standard electronics and data acquisition systems were used in connection with the detectors. A 50 Hz pulser was stored concurrently in the spectra to monitor dead time effects, which were kept below 10%.

In order to minimise the effects of multiple scattering on the observed scattering yields [16,36], the targets had to be thin, e.g. less than 10 μg/cm^2. This condition prevented the use of self-supporting solid targets; instead thin targets on a suitable backing had to be used. Furthermore, to arrive at a sufficient energy resolution - in particular at low beam energies - between the elastic scattering signals from the thin target and the (infinitely) thick backing, the masses of the target and backing nuclides had to be quite different. This led to the choice of Ta and W targets vacuum-evaporated on Si backings. Other alternative backings such as Al or saphir (Al_2O_3) were dismissed [31] due to lack of sufficient cleanliness of the backings in comparison to commercial Si wafers (Fig. 1). Due to the high melting temperature of Ta and W, these target materials had to be vacuum-evaporated in form of Ta_2O_5 (≈ 2.5 μg/cm^2, from measurements using a quartz-oscillator) and WO_3 (≈ 5.0 μg/cm^2). Alternative targets such as Ag, Au, Pb and Pt were dismissed due to a higher target deterioration during ^{4}He bombardment e.g. via the sputtering effects [31]. An Al-Au sandwich target (both of 5 μg/cm^2 thickness) on an Al backing was also dismissed due to uncertainties in thickness of the sputtered Al-layer.

Since thin targets can have significant inhomogeneities (more than 10%) due to the formation of islands [31], the ion beam was scanned over the target area using 2 magnetic steerers placed in front of the apertures A_1 and A_2; the horizontal and vertical steerers were operated with different frequencies (5.2 and 7.0 Hz) and their deflect-

ing amplitudes were chosen such that the final beam current on target was reduced by a factor of 2. The stability of the targets was monitored at the reference energy E_{lab} = 900 keV. The Ta_2O_5 and WO_3 targets deteriorated both by about 1% over a running time of 1 week [31]; this deterioration was taken into account in the analysis of the data. The signals from the target and Si substrate were clearly resolved at $E_{lab} \geq 250$ keV (Fig. 1) and the respective line-shapes were determined as a function of beam energy. The results were used to analyse the spectra at the lowest energies, i.e. $E_{lab} = 76.1$ to 200 keV, where both signals partially overlapped (Fig. 1). Slight variations of the fit-parameters were used to estimate the resulting uncertainty in $N(E,\theta)$. At the lowest beam energy the correction due to convolution of the target peak with the Si substrate was approximately 6% (uncertainty = 2.5%). This correction quickly decreased to less than 2% (uncertainty $\leq$ 0.5%) with increasing beam energy, and for most data the correction due to tailing of the target peak yield underneath the Si substrate yield was less than 1% and neglected.

Finally, the observed yields have to be corrected for the effects of backscattering directly from the surface-barrier detector window without producing any signal in the detector active volume. We used TRIM simulations [33] to estimate the effects: the detector efficiency corrections decreased quickly with increasing energy, and typical corrections were less than 0.1% at all but the lowest energies, where the correction approached 1.2%. The number of target atoms, N_t, was determined at the highest energy, $E_{lab} = 3.988$ MeV, where the effects of electron screening are negligible (less than 0.8%). Thus, assuming $\sigma(E,\theta) = \sigma_R(E,\theta)$ at E_{lab} = 3.988 MeV, we obtained with equation 3: $N_t = (1.19 \pm 0.05) \cdot 10^{16}$ Ta-atoms/cm^2 and $(1.55 \pm 0.05) \cdot 10^{16}$ W-atoms/cm^2, leading to $N_t(Ta_2O_5) = 4.36$ μg/cm^2 and $N_t(WO_3) = 5.97$ μg/cm^2.

Multiple scattering effects [16,36] lead to an increase of the differential cross section, in particular at low beam energies. For the targets used, the correction was estimated to be less than 1%, even at the lowest energy (E_{lab} = 76.1 keV), and was neglected. The vacuum polarisation [26,34] increases also the differential cross section for high energies, leading to a correction of less than 0.5% in all cases, which was also neglected. Similarly, the relativistic correction [26] is negligibly small (less than 0.05%). The ratio of number of counts extracted for the two 165° detectors over the entire energy range was found to be 1.009 (on average) with a standard deviation of 0.01. The average value indicates a precision in geometry of about 0.8%; the standard deviation is consistent with the angle spread of 1°. With the knowledge of the target thickness and the use of stopping power compilations [33] the energy loss in the target, Δ_{lab}, was calculated, e.g. Δ_{lab} = 1.56 keV for the WO_3 target at the lowest energy, E_{lab} = 76.1 keV. The effective energy within the target [2] was taken here as that corresponding to one-half the target thickness, thus $E = 73.72 \pm 0.08$ keV, where the error corresponds to an assumed 10% uncertainty in the stopping power values. The error in E leads to a negligible uncertainty of 0.2% in $\sigma(E,\theta)$. In summary, many factors influenced the ultimate relative error of the present measurements. Firstly, there are errors common to all data points: current integration (0.35%), loss of secondary electrons (0.9%), deterioration/variation of target thickness (1%), beam neutrals (0.5%), beam direction (0.08%) and normalisation (5%). Adding these uncertainties in quadratures, one arrives at a common error of 5.2% for all data points. Secondly, there are errors associated with each data point: counting statistics ($\leq$ 1%), mean energy at one-half the target thickness ($\leq$ 0.2%), incident beam energy ($\leq$ 1.1%), target peak convolution ($\leq$ 2.5%), and detector efficiency ($\leq$ 1.2%). Adding these uncertainties in quadratures, the resulting error is given in Table 1 for each data point.

3 Results and discussion

The resulting screening factors,

$$f_{lab}(E,\theta) = \sigma(E,\theta)/\sigma_R(E,\theta),$$

for both scattering systems are summarised in Table 1 and displayed in Fig. 2. The results were fitted using equation (6) leading to values for the electron screening potential energy $U_e = 30.5 \pm 4.5$ keV ($\chi^2 = 0.67$) and $U_e = 25.7 \pm 4.4$ keV ($\chi^2 = 0.72$) for the He+Ta and He+W scattering systems, respectively, with an average value of $U_e = 28 \pm 3$ keV. The deduced U_e values for both scattering systems are identical within experimental error, as one may expect from the small difference in nuclear charge between Ta ($Z = 73$) and W ($Z = 74$).

It has been suggested [e.g. 35] that for energies far below the height of the Coulomb barrier the elastic scattering of ions by atoms can be described by a screened Coulomb potential,

$$V(r) = Z_1 Z_2 e^2 r^{-1} \phi(r/a), \tag{7}$$

where a is the screening radius and ϕ(r/a) is the screening function. For the screening radius the following expression was derived [35]:

$$a = 0.885 a_o (Z_1^{2/3} + Z_2^{2/3})^{-1/2}, \tag{8}$$

where a_o is the Bohr radius. For the screening function various forms have been proposed:

"Bohr" [36]:

$$\phi(r/a) = \exp(-\mathrm{r/a}). \tag{9}$$

"Moliére" [37]:

$$\phi(r/a) = 0.35\exp(-0.3\mathrm{r/a}) + 0.55\exp(-1.2\mathrm{r/a}) + 0.1\exp(-6.0\mathrm{r/a}). \tag{10}$$

"Wilson" [38]:

$$\phi(r/a) = 0.0069\exp(-0.13\mathrm{r/a}) + 0.17\exp(-0.31\mathrm{r/a}) + 0.83\exp(-0.92\mathrm{r/a}). \tag{11}$$

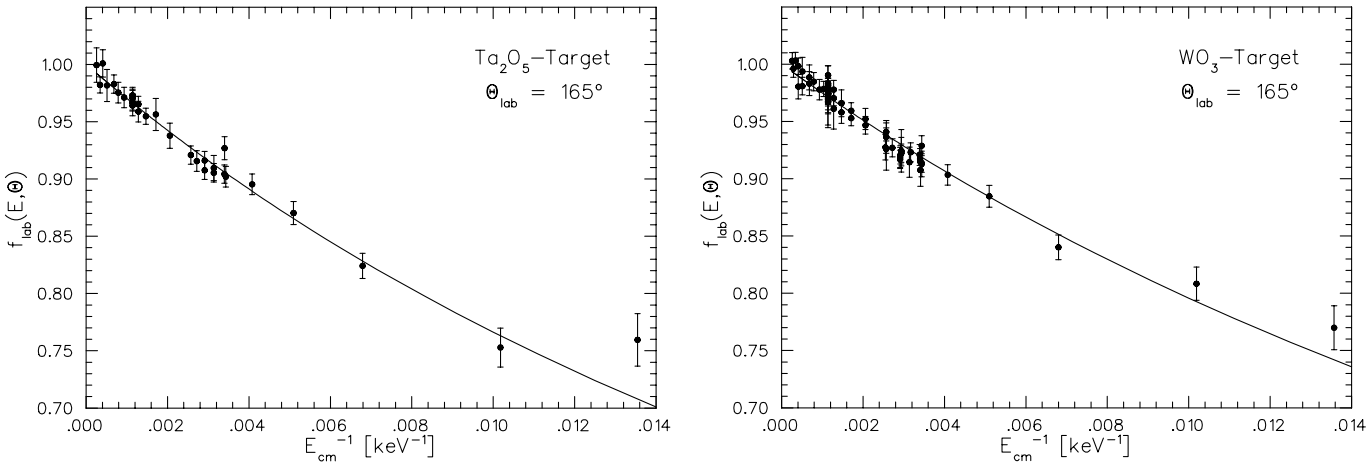

Fig. 2. Differential cross section relativ to the Rutherford scattering law for the He+Ta and He+W scattering systems at $\theta_{lab} = 165^\circ$ is shown as a function of inverse-center-of mass energy E. The solid curves represent the results of a fit using eq. 6

Table 1. Differential cross section relative to the Rutherford scattering law, $f_{lab}(E,\theta) = \sigma(E,\theta)/\sigma_R(E,\theta)$, at $\theta_{lab} = 165^\circ$.

Ta_2O_5 target		WO_3 target	
$E[keV]$[a]	$f_{lab}(E,\theta)$[b]	$E[keV]$[a]	$f_{lab}(E,\theta)$[b]
73.8	0.760 ± 0.023	73.7	0.770 ± 0.019
98.3	0.753 ± 0.017	98.2	0.808 ± 0.015
147.2	0.824 ± 0.011	147.0	0.840 ± 0.011
196.3	0.870 ± 0.010	195.9	0.885 ± 0.010
245.3	0.895 ± 0.009	245.0	0.903 ± 0.009
291.4	0.902 ± 0.009	291.0	0.919 ± 0.011
294.1	0.915 ± 0.008	293.3	0.913 ± 0.014
318.9	0.907 ± 0.008	293.9	0.917 ± 0.009
343.4	0.912 ± 0.008	294.9	0.921 ± 0.009
368.0	0.916 ± 0.009	315.4	0.923 ± 0.013
388.8	0.921 ± 0.008	318.5	0.914 ± 0.013
486.3	0.938 ± 0.011	339.7	0.923 ± 0.013
583.8	0.956 ± 0.014	343.0	0.920 ± 0.009
681.3	0.955 ± 0.007	344.2	0.917 ± 0.008
778.8	0.962 ± 0.008	367.4	0.927 ± 0.008
876.3	0.969 ± 0.007	388.5	0.934 ± 0.014
1071	0.971 ± 0.009	392.1	0.927 ± 0.011
1266	0.975 ± 0.009	485.9	0.948 ± 0.009
1462	0.983 ± 0.008	583.3	0.956 ± 0.007
1949	0.982 ± 0.014	680.9	0.962 ± 0.012
2437	1.001 ± 0.012	778.4	0.970 ± 0.008
2925	0.982 ± 0.007	872.0	0.975 ± 0.007
3901	1.000 ± 0.015	876.0	0.981 ± 0.008
		973.6	0.978 ± 0.007
		1071	0.978 ± 0.009
		1266	0.985 ± 0.008
		1462	0.986 ± 0.010
		1949	0.987 ± 0.010
		2437	0.989 ± 0.010
		2926	1.003 ± 0.007
		3414	0.996 ± 0.008
		3902	1.003 ± 0.007

[a] Effective center-of-mass energy

[b] The quoted errors include in quadratures the individual errors of each data point (see text). A common error of 5.2% has to be added to the quoted values

"Lenz-Jensen" [39,40]:

$$\phi(r/a) = \exp(-y)(1 + y + 0.33y^2 + 0.049y^3 + 0.0027y^4)$$
$$\text{with } y = (9.7r/a)^{1/2}. \quad (12)$$

"Ziegler" [41]:

$$\phi(r/a) = 0.18\exp(-3.2r/a) + 0.51\exp(-0.94r/a) + 0.28\exp(-0.40r/a) + 0.028\exp(-0.20r/a)$$
$$(\text{here : } a = 0.885a_o(Z_1^{0.23} + Z_2^{0.23})^{-1}). \quad (13)$$

Using first-order expansion of $\phi(r/a)$ the screening potential energy U_e is given approximately by the expression

$$U_e = -Z_1 Z_2 e^2 a^{-1} \phi'(0). \quad (14)$$

With $Z_1 Z_2 e^2 a^{-1} = 19.3$ and 19.9 keV for the He+Ta and He+W scattering systems, respectively and the averaged value of 19.6 keV, the observed average value $U_e = 28 \pm 3$ keV leads to $\phi'(0) = -1.43 \pm 0.15$. In comparison, the suggested screening functions lead to $\phi'(0) = -1.0, -1.37, -0.81, -1.60$, and -1.18 for the Bohr-, Moliére-, Wilson-, Lenz-Jensen-, and Ziegler-ansatz, respectively, thus favoring the Moliére- and Lenz-Jensen-forms.

From the difference in atomic binding energies between projectile plus target and compound atom - deduced from relativistic Hartree-Fock-Slater eigenvalues [42] - one finds $U_e = 30.0$ keV, in good agreement with observation. Thus, one may conclude that the observed electron screening effects in the elastic scattering process are fully consistent with atomic physics models, at least for heavy scattering systems. However, the conclusion might not be applicable for light scattering systems such as H+He and He+He (Sect. 1), where shell effects of the atomic clouds might be important. Experimental studies of the electron screening effects in such systems demand for measurements down to energies far below 1 keV, a great challenge to the experimentalists.

The authors would like to thank K. Langanke and F. Besenbacher (Aarhus University) for comments on the manuscript.

References

1. W.A. Fowler, Rev. Mod. Phys. **56** (1984) 149
2. C. Rolfs and W.S. Rodney, Cauldrons in the Cosmos (University of Chicago Press, 1988)
3. H.J. Assenbaum, K. Langanke and C. Rolfs, Z. Phys. A**327** (1987) 461
4. S. Engstler, A. Krauss, K. Neldner, C. Rolfs, U. Schröder and K. Langanke, Phys. Lett. B**202** (1988) 179
5. S. Engstler, G. Raimann, C. Angulo, U. Greife, C. Rolfs, U. Schröder, E. Somorjai, B. Kirch and K. Langanke, Phys. Lett. B**279** (1992) 20 and Z. Phys. A**342** (1992) 471
6. C. Angulo, S. Engstler, G. Raimann, C. Rolfs, W.H. Schulte and E. Somorjai, Z. Phys. A**345** (1993) 231
7. P. Prati, C. Arpesella, F. Bartolucci, H.W. Becker, E. Bellotti, C. Broggini, P. Corvisiero, G. Fiorentini, S. Fubini, G. Gervino, F. Gorris, U. Greife, C. Gustavino, M. Junker, C. Rolfs, W. H. Schulte, H. P. Trautvetter and D. Zahnow , Z. Phys. A**350** (1994) 171
8. U. Greife, F. Gorris, M. Junker, C. Rolfs and D. Zahnow, Z. Phys. A**351** (1995) 107
9. D. Zahnow, C. Rolfs, S. Schmidt and H. P. Trautvetter, Z. Phys. A**359** (1997) 211
10. C. Arpesella, E. Bellotti, C. Broggini, P. Corvisiero, S. Fubini, G. Gervino, U. Greife, C. Gustavino, M. Junker, A. Lanza, P. Prati, C. Rolfs, D. Zahnow and S. Zavatarelli, Phys. Lett. B**389** (1996) 452 and Phys. Rev. (in press)
11. G. Fiorentini, R. W. Kavanagh and C. Rolfs, Z. Phys. A**350** (1995) 289.
12. C. Rolfs and E. Somorjai, Nucl. Instr. Meth. B**99** (1995) 297
13. L. Bracci, G. Fiorentini, V. S. Melezhik, G. Mezzorani and P. Quarati, Nucl. Phys. A**513** (1990) 316
14. T. D. Shoppa, S. E. Koonin, K. Langanke and R. Seki, Phys. Rev. C**48** (1993) 837
15. K. Langanke, T. D. Shoppa, C. A. Barnes and C. Rolfs, Phys. Lett. B**369** (1996) 211
16. A. van Wijngaarden, E. J. Brimner and W. E. Baylis, Can. J. Phys. **48** (1970) 1835
17. A. van Wijngaarden and W. E. Baylis, Phys. Rev. A**7** (1973) 937
18. H. J. Goldberg, H. E. Jach and E. B. Dale, Phys. Rev. A**12** (1975) 908
19. W. F. S. Poehlman, D. A. Thompson and J. A. Davies, Nucl. Instr. Meth. **191** (1981) 495
20. S.R. Lee and R.R. Hart, Nucl. Instr. Meth. B**79** (1993) 463
21. H.H. Andersen, J. Bottiger and H. Knudsen, Phys. Rev. A**7** (1973) 154
22. H.H. Andersen and H. Knudsen, Phys. Rev. A**10** (1974) 733
23. H. Knudsen and P. Moller-Petersen, Radiat. Eff. **28** (1976) 147 and J. Phys. B**11** (1978) 455
24. J. L'Ecuyer, J. A. Davies and N. Matsunami, Nucl. Instr. Meth. **160** (1979) 337
25. P. Loftager, F. Besenbacher, O. S. Jensen and V. S. Soerensen, Phys. Rev. A**20** (1979) 1443
26. H. H. Andersen, F. Besenbacher, P. Loftager and W. Möller, Phys. Rev. A**21** (1980) 1891
27. M. Hautala and M. Luomajarvi, Radiat. Eff. **45** (1980) 159
28. A. Weber, H. Dahlmann, H. Mommsen and W. Sarter, Nucl. Instr. Meth. **200** (1982) 567
29. E. Huttel, W. Arnold, H. Baumgart and G. Clausnitzer, Nucl. Instr. Meth. B**12** (1985) 193
30. R. Golser, D. Semrad and P. Bauer, Nucl. Instr. Meth. B**28** (1987) 311
31. F. Schümann, Diplomarbeit, Ruhr-Universität Bochum (1997)
32. H. W. Becker, M. Bahr, M. Berheide, L. Borucki, M. Buschmann, C. Rolfs, G. Roters, S. Schmidt, W. H. Schulte, G. E. Mitchell and J. S. Schweitzer, Z. S. Schmidt, Z. Phys. A**351** (1995) 453
33. TRIM program "Transport of Ions in Matter (version 1-98)
34. L. Durand, Phys. Rev. **108** (1957) 1597
35. J. Lindhard, V. Nielsen and M. Scharff , Kg. Dan. Vid. Selsk. Mat. Fys. Medd. **36** (1968) 10
36. N. Bohr, Kg. Dan. Vid. Selsk. Mat. Fys. Medd. **18** (1948) 8
37. G. Moliére, Zeitsch. Naturf. **2a** (1947) 133
38. W. D. Wilson, L. G. Haggmark and J. P. Biersack, Phys. Rev. **15** (1977) 2458
39. W. Lenz, Z. Phys. **77** (1932) 713
40. H. Jensen, Z. Phys. **77** (1932) 722
41. J. F. Ziegler, J. P. Biersack and U. Littmark, The Stopping and Range of Ions in Solids (Pergamon, New York, 1985)
42. C. C. Lu, T. A. Carlson, F. B. Malik, T. C. Tucker and C. W. Nestor, Atomic Data **3** (1971) 1